

# Centrality Dependence of the High $p_T$ Charged Hadron Suppression in Au+Au Collisions at $\sqrt{s_{NN}} = 130$ GeV

K. Adcox,<sup>40</sup> S. S. Adler,<sup>3</sup> N. N. Ajitanand,<sup>27</sup> Y. Akiba,<sup>14</sup> J. Alexander,<sup>27</sup> L. Aphecetche,<sup>34</sup> Y. Arai,<sup>14</sup> S. H. Aronson,<sup>3</sup> R. Averbeck,<sup>28</sup> T. C. Awes,<sup>29</sup> K. N. Barish,<sup>5</sup> P. D. Barnes,<sup>19</sup> J. Barrette,<sup>21</sup> B. Bassalleck,<sup>25</sup> S. Bathe,<sup>22</sup> V. Baublis,<sup>30</sup> A. Bazilevsky,<sup>12,32</sup> S. Belikov,<sup>12,13</sup> F. G. Bellaiche,<sup>29</sup> S. T. Belyaev,<sup>16</sup> M. J. Bennett,<sup>19</sup> Y. Berdnikov,<sup>35</sup> S. Botelho,<sup>33</sup> M. L. Brooks,<sup>19</sup> D. S. Brown,<sup>26</sup> N. Bruner,<sup>25</sup> D. Bucher,<sup>22</sup> H. Buesching,<sup>22</sup> V. Bumazhnov,<sup>12</sup> G. Bunce,<sup>3,32</sup> J. Burward-Hoy,<sup>28</sup> S. Butsyk,<sup>28,30</sup> T. A. Carey,<sup>19</sup> P. Chand,<sup>2</sup> J. Chang,<sup>5</sup> W. C. Chang,<sup>1</sup> L. L. Chavez,<sup>25</sup> S. Chernichenko,<sup>12</sup> C. Y. Chi,<sup>8</sup> J. Chiba,<sup>14</sup> M. Chiu,<sup>8</sup> R. K. Choudhury,<sup>2</sup> T. Christ,<sup>28</sup> T. Chujo,<sup>3,39</sup> M. S. Chung,<sup>15,19</sup> P. Chung,<sup>27</sup> V. Cianciolo,<sup>29</sup> B. A. Cole,<sup>8</sup> D. G. D'Enterria,<sup>34</sup> G. David,<sup>3</sup> H. Delagrange,<sup>34</sup> A. Denisov,<sup>12</sup> A. Deshpande,<sup>32</sup> E. J. Desmond,<sup>3</sup> O. Dietzsch,<sup>33</sup> B. V. Dinesh,<sup>2</sup> A. Drees,<sup>28</sup> A. Durum,<sup>12</sup> D. Dutta,<sup>2</sup> K. Ebisu,<sup>24</sup> Y. V. Efremenko,<sup>29</sup> K. El Chenawi,<sup>40</sup> H. En'yo,<sup>17,31</sup> S. Esumi,<sup>39</sup> L. Ewell,<sup>3</sup> T. Ferdousi,<sup>5</sup> D. E. Fields,<sup>25</sup> S. L. Fokin,<sup>16</sup> Z. Fraenkel,<sup>42</sup> A. Franz,<sup>3</sup> A. D. Frawley,<sup>9</sup> S. -Y. Fung,<sup>5</sup> S. Garpman,<sup>20,\*</sup> T. K. Ghosh,<sup>40</sup> A. Glenn,<sup>36</sup> A. L. Godoi,<sup>33</sup> Y. Goto,<sup>32</sup> S. V. Greene,<sup>40</sup> M. Grosse Perdekamp,<sup>32</sup> S. K. Gupta,<sup>2</sup> W. Guryn,<sup>3</sup> H. -Å. Gustafsson,<sup>20</sup> J. S. Haggerty,<sup>3</sup> H. Hamagaki,<sup>7</sup> A. G. Hansen,<sup>19</sup> H. Hara,<sup>24</sup> E. P. Hartouni,<sup>18</sup> R. Hayano,<sup>38</sup> N. Hayashi,<sup>31</sup> X. He,<sup>10</sup> T. K. Hemmick,<sup>28</sup> J. M. Heuser,<sup>28</sup> M. Hibino,<sup>41</sup> J. C. Hill,<sup>13</sup> D. S. Ho,<sup>43</sup> K. Homma,<sup>11</sup> B. Hong,<sup>15</sup> A. Hoover,<sup>26</sup> T. Ichihara,<sup>31,32</sup> K. Imai,<sup>17,31</sup> M. S. Ippolitov,<sup>16</sup> M. Ishihara,<sup>31,32</sup> B. V. Jacak,<sup>28,32</sup> W. Y. Jang,<sup>15</sup> J. Jia,<sup>28</sup> B. M. Johnson,<sup>3</sup> S. C. Johnson,<sup>18,28</sup> K. S. Joo,<sup>23</sup> S. Kametani,<sup>41</sup> J. H. Kang,<sup>43</sup> M. Kann,<sup>30</sup> S. S. Kapoor,<sup>2</sup> S. Kelly,<sup>8</sup> B. Khachaturov,<sup>42</sup> A. Khanzadeev,<sup>30</sup> J. Kikuchi,<sup>41</sup> D. J. Kim,<sup>43</sup> H. J. Kim,<sup>43</sup> S. Y. Kim,<sup>43</sup> Y. G. Kim,<sup>43</sup> W. W. Kinnison,<sup>19</sup> E. Kistenev,<sup>3</sup> A. Kiyomichi,<sup>39</sup> C. Klein-Boesing,<sup>22</sup> S. Klinksiek,<sup>25</sup> L. Kochenda,<sup>30</sup> V. Kochetkov,<sup>12</sup> D. Koehler,<sup>25</sup> T. Kohama,<sup>11</sup> D. Kotchetkov,<sup>5</sup> A. Kozlov,<sup>42</sup> P. J. Kroon,<sup>3</sup> K. Kurita,<sup>31,32</sup> M. J. Kweon,<sup>15</sup> Y. Kwon,<sup>43</sup> G. S. Kyle,<sup>26</sup> R. Lacey,<sup>27</sup> J. G. Lajoie,<sup>13</sup> J. Lauret,<sup>27</sup> A. Lebedev,<sup>13,16</sup>

D. M. Lee,<sup>19</sup> M. J. Leitch,<sup>19</sup> X. H. Li,<sup>5</sup> Z. Li,<sup>6,31</sup> D. J. Lim,<sup>43</sup> M. X. Liu,<sup>19</sup> X. Liu,<sup>6</sup> Z. Liu,<sup>6</sup> C. F. Maguire,<sup>40</sup> J. Mahon,<sup>3</sup> Y. I. Makdisi,<sup>3</sup> V. I. Manko,<sup>16</sup> Y. Mao,<sup>6,31</sup> S. K. Mark,<sup>21</sup> S. Markacs,<sup>8</sup> G. Martinez,<sup>34</sup> M. D. Marx,<sup>28</sup> A. Masaike,<sup>17</sup> F. Matathias,<sup>28</sup> T. Matsumoto,<sup>7,41</sup> P. L. McGaughey,<sup>19</sup> E. Melnikov,<sup>12</sup> M. Merschmeyer,<sup>22</sup> F. Messer,<sup>28</sup> M. Messer,<sup>3</sup> Y. Miake,<sup>39</sup> T. E. Miller,<sup>40</sup> A. Milov,<sup>42</sup> S. Mioduszewski,<sup>3,36</sup> R. E. Mischke,<sup>19</sup> G. C. Mishra,<sup>10</sup> J. T. Mitchell,<sup>3</sup> A. K. Mohanty,<sup>2</sup> D. P. Morrison,<sup>3</sup> J. M. Moss,<sup>19</sup> F. Mühlbacher,<sup>28</sup> M. Muniruzzaman,<sup>5</sup> J. Murata,<sup>31</sup> S. Nagamiya,<sup>14</sup> Y. Nagasaka,<sup>24</sup> J. L. Nagle,<sup>8</sup> Y. Nakada,<sup>17</sup> B. K. Nandi,<sup>5</sup> J. Newby,<sup>36</sup> L. Nikkinen,<sup>21</sup> P. Nilsson,<sup>20</sup> S. Nishimura,<sup>7</sup> A. S. Nyanin,<sup>16</sup> J. Nystrand,<sup>20</sup> E. O'Brien,<sup>3</sup> C. A. Ogilvie,<sup>13</sup> H. Ohnishi,<sup>3,11</sup> I. D. Ojha,<sup>4,40</sup> M. Ono,<sup>39</sup> V. Onuchin,<sup>12</sup> A. Oskarsson,<sup>20</sup> L. Österman,<sup>20</sup> I. Otterlund,<sup>20</sup> K. Oyama,<sup>7,38</sup> L. Paffrath,<sup>3,\*</sup> A. P. T. Palounek,<sup>19</sup> V. S. Pantuev,<sup>28</sup> V. Papavassiliou,<sup>26</sup> S. F. Pate,<sup>26</sup> T. Peitzmann,<sup>22</sup> A. N. Petridis,<sup>13</sup> C. Pinkenburg,<sup>3,27</sup> R. P. Pisani,<sup>3</sup> P. Pitukhin,<sup>12</sup> F. Plasil,<sup>29</sup> M. Pollack,<sup>28,36</sup> K. Pope,<sup>36</sup> M. L. Purschke,<sup>3</sup> I. Ravinovich,<sup>42</sup> K. F. Read,<sup>29,36</sup> K. Reygers,<sup>22</sup> V. Riabov,<sup>30,35</sup> Y. Riabov,<sup>30</sup> M. Rosati,<sup>13</sup> A. A. Rose,<sup>40</sup> S. S. Ryu,<sup>43</sup> N. Saito,<sup>31,32</sup> A. Sakaguchi,<sup>11</sup> T. Sakaguchi,<sup>7,41</sup> H. Sako,<sup>39</sup> T. Sakuma,<sup>31,37</sup> V. Samsonov,<sup>30</sup> T. C. Sangster,<sup>18</sup> R. Santo,<sup>22</sup> H. D. Sato,<sup>17,31</sup> S. Sato,<sup>39</sup> S. Sawada,<sup>14</sup> B. R. Schlei,<sup>19</sup> Y. Schutz,<sup>34</sup> V. Semenov,<sup>12</sup> R. Seto,<sup>5</sup> T. K. Shea,<sup>3</sup> I. Shein,<sup>12</sup> T.-A. Shibata,<sup>31,37</sup> K. Shigaki,<sup>14</sup> T. Shiina,<sup>19</sup> Y. H. Shin,<sup>43</sup> I. G. Sibiriak,<sup>16</sup> D. Silvermyr,<sup>20</sup> K. S. Sim,<sup>15</sup> J. Simon-Gillo,<sup>19</sup> C. P. Singh,<sup>4</sup> V. Singh,<sup>4</sup> M. Sivertz,<sup>3</sup> A. Soldatov,<sup>12</sup> R. A. Soltz,<sup>18</sup> S. Sorensen,<sup>29,36</sup> P. W. Stankus,<sup>29</sup> N. Starinsky,<sup>21</sup> P. Steinberg,<sup>8</sup> E. Stenlund,<sup>20</sup> A. Ster,<sup>44</sup> S. P. Stoll,<sup>3</sup> M. Sugioka,<sup>31,37</sup> T. Sugitate,<sup>11</sup> J. P. Sullivan,<sup>19</sup> Y. Sumi,<sup>11</sup> Z. Sun,<sup>6</sup> M. Suzuki,<sup>39</sup> E. M. Takagui,<sup>33</sup> A. Takeuchi,<sup>31</sup> M. Tamai,<sup>41</sup> K. H. Tanaka,<sup>14</sup> Y. Tanaka,<sup>24</sup> E. Taniguchi,<sup>31,37</sup> M. J. Tannenbaum,<sup>3</sup> J. Thomas,<sup>28</sup> J. H. Thomas,<sup>18</sup> T. L. Thomas,<sup>25</sup> W. Tian,<sup>6,36</sup> J. Tojo,<sup>17,31</sup> H. Torii,<sup>17,31</sup> R. S. Towell,<sup>19</sup> I. Tserruya,<sup>42</sup> H. Tsuruoka,<sup>39</sup> A. A. Tsvetkov,<sup>16</sup> S. K. Tuli,<sup>4</sup> H. Tydesjö,<sup>20</sup> N. Tyurin,<sup>12</sup> T. Ushiroda,<sup>24</sup> H. W. van Hecke,<sup>19</sup> C. Velissaris,<sup>26</sup> J. Velkovska,<sup>28</sup> M. Velkovsky,<sup>28</sup> A. A. Vinogradov,<sup>16</sup> M. A. Volkov,<sup>16</sup> A. Vorobyov,<sup>30</sup> E. Vznuzdaev,<sup>30</sup> H. Wang,<sup>5</sup> Y. Watanabe,<sup>31,32</sup> S. N. White,<sup>3</sup> C. Witzig,<sup>3</sup> F. K. Wohn,<sup>13</sup> C. L. Woody,<sup>3</sup> W. Xie,<sup>5,42</sup> K. Yagi,<sup>39</sup> S. Yokkaichi,<sup>31</sup> G. R. Young,<sup>29</sup> I. E. Yushmanov,<sup>16</sup> W. A. Zajc,<sup>8</sup>

Z. Zhang,<sup>28</sup> and S. Zhou<sup>6</sup>

(PHENIX Collaboration)

<sup>1</sup>*Institute of Physics, Academia Sinica, Taipei 11529, Taiwan*

<sup>2</sup>*Bhabha Atomic Research Centre, Bombay 400 085, India*

<sup>3</sup>*Brookhaven National Laboratory, Upton, NY 11973-5000, USA*

<sup>4</sup>*Department of Physics, Banaras Hindu University, Varanasi 221005, India*

<sup>5</sup>*University of California - Riverside, Riverside, CA 92521, USA*

<sup>6</sup>*China Institute of Atomic Energy (CIAE), Beijing, People's Republic of China*

<sup>7</sup>*Center for Nuclear Study, Graduate School of Science, University of Tokyo, 7-3-1 Hongo, Bunkyo, Tokyo 113-0033, Japan*

<sup>8</sup>*Columbia University, New York, NY 10027 and Nevis Laboratories, Irvington, NY 10533, USA*

<sup>9</sup>*Florida State University, Tallahassee, FL 32306, USA*

<sup>10</sup>*Georgia State University, Atlanta, GA 30303, USA*

<sup>11</sup>*Hiroshima University, Kagamiyama, Higashi-Hiroshima 739-8526, Japan*

<sup>12</sup>*Institute for High Energy Physics (IHEP), Protvino, Russia*

<sup>13</sup>*Iowa State University, Ames, IA 50011, USA*

<sup>14</sup>*KEK, High Energy Accelerator Research Organization, Tsukuba-shi, Ibaraki-ken 305-0801, Japan*

<sup>15</sup>*Korea University, Seoul, 136-701, Korea*

<sup>16</sup>*Russian Research Center "Kurchatov Institute", Moscow, Russia*

<sup>17</sup>*Kyoto University, Kyoto 606, Japan*

<sup>18</sup>*Lawrence Livermore National Laboratory, Livermore, CA 94550, USA*

<sup>19</sup>*Los Alamos National Laboratory, Los Alamos, NM 87545, USA*

<sup>20</sup>*Department of Physics, Lund University, Box 118, SE-221 00 Lund, Sweden*

<sup>21</sup>*McGill University, Montreal, Quebec H3A 2T8, Canada*

<sup>22</sup>*Institut für Kernphysik, University of Münster, D-48149 Münster, Germany*

<sup>23</sup>*Myongji University, Yongin, Kyonggido 449-728, Korea*

<sup>24</sup>*Nagasaki Institute of Applied Science, Nagasaki-shi, Nagasaki 851-0193, Japan*

<sup>25</sup>*University of New Mexico, Albuquerque, NM 87131, USA*

<sup>26</sup>*New Mexico State University, Las Cruces, NM 88003, USA*

<sup>27</sup>*Chemistry Department, State University of New York - Stony Brook, Stony Brook, NY 11794, USA*

<sup>28</sup>*Department of Physics and Astronomy, State University of New York - Stony Brook, Stony Brook, NY 11794, USA*

<sup>29</sup>*Oak Ridge National Laboratory, Oak Ridge, TN 37831, USA*

<sup>30</sup>*PNPI, Petersburg Nuclear Physics Institute, Gatchina, Russia*

<sup>31</sup>*RIKEN (The Institute of Physical and Chemical Research), Wako, Saitama 351-0198, JAPAN*

<sup>32</sup>*RIKEN BNL Research Center, Brookhaven National Laboratory, Upton, NY 11973-5000, USA*

<sup>33</sup>*Universidade de São Paulo, Instituto de Física, Caixa Postal 66318, São Paulo CEP05315-970, Brazil*

<sup>34</sup>*SUBATECH (Ecole des Mines de Nantes, IN2P3/CNRS, Universite de Nantes) BP 20722 - 44307, Nantes-cedex 3, France*

<sup>35</sup>*St. Petersburg State Technical University, St. Petersburg, Russia*

<sup>36</sup>*University of Tennessee, Knoxville, TN 37996, USA*

<sup>37</sup>*Department of Physics, Tokyo Institute of Technology, Tokyo, 152-8551, Japan*

<sup>38</sup>*University of Tokyo, Tokyo, Japan*

<sup>39</sup>*Institute of Physics, University of Tsukuba, Tsukuba, Ibaraki 305, Japan*

<sup>40</sup>*Vanderbilt University, Nashville, TN 37235, USA*

<sup>41</sup>*Waseda University, Advanced Research Institute for Science and Engineering, 17 Kikui-cho, Shinjuku-ku, Tokyo 162-0044, Japan*

<sup>42</sup>*Weizmann Institute, Rehovot 76100, Israel*

<sup>43</sup>*Yonsei University, IPAP, Seoul 120-749, Korea*

<sup>44</sup>*KFKI Research Institute for Particle and Nuclear Physics (RMKI), Budapest, Hungary<sup>†</sup>*

(February 11, 2019)

## Abstract

PHENIX has measured the centrality dependence of charged hadron  $p_T$  spectra from central Au+Au collisions at  $\sqrt(s_{NN}) = 130$  GeV. The local inverse slope decreases with centrality for  $p_T > 2$  GeV/c, indicating an apparent reduction of the contribution from hard scattering to high  $p_T$  hadron production. For central collisions the yield at high  $p_T$  is shown to be suppressed compared binary collision scaling of p+p data. The suppression sets in over the centrality range 30-60%, corresponding to about 40-140 participating nucleons. The observed  $p_T$  and centrality dependence is consistent with the particle production predicted by models including hard scattering and subsequent energy loss of the scattered partons in the dense matter created in the collisions.

PACS numbers: 25.75.Dw

## I. INTRODUCTION

Particle production at large transverse momentum ( $p_T$ ) provides an important new tool to study the hot and dense nuclear matter created in high energy nuclear collisions at the Brookhaven National Laboratory Relativistic Heavy Ion Collider (RHIC) facility. In nucleon-nucleon collisions at collider energies, particles with  $p_T \geq 2$  GeV/c originate mostly from the fragmentation of hard scattered partons [1]. Because of the large  $Q^2$  of hard scattering processes the outgoing partons are thought to be the first particles “born” in a nuclear collision at RHIC. As a result, they traverse the highest energy density matter produced in nuclear collisions. Theoretical studies of the propagation of quarks and gluons in such matter suggest that they may lose a significant fraction of their energy through gluon bremsstrahlung [2] and that the amount of energy loss depends directly on the density of color charges in the matter through which the partons pass [3]. The resulting reduction in the parton momenta would produce a corresponding reduction in the momenta of the fragmentation products and thus would reduce the yield of hadrons in a fixed  $p_T$  range relative to the yield observed in nucleon-nucleon collisions multiplied by the number of binary nucleon-nucleon collisions [4].

The first measurements of hadron spectra at high  $p_T$  at RHIC have indeed indicated a suppression of high- $p_T$  hadron production in central Au+Au collisions relative to a binary-collision scaling of p+p and  $\bar{p}+p$  data [5]. In the same data-set, no suppression is found for peripheral Au+Au collisions. Calculations of the effects of parton energy loss on the spectrum of high- $p_T$  hadrons in perturbative QCD-inspired models can reproduce the observed suppression in central Au+Au collisions while simultaneously describing the peripheral data were no suppression is found [6,7,9]. If the suppression is due to energy loss by medium-induced gluon radiation, then systematic measurements of high- $p_T$  hadron spectra might directly probe the color charge density or more generally the opacity [7] of the matter produced early in a RHIC collision.

However, there are other possible ways to produce a suppression in the  $p_T$  range covered

by the published data. A recent analysis of the re-scattering of hadrons originally produced via the fragmentation of a high- $p_T$  parton suggest that the resulting energy degradation could be sufficient to describe the high- $p_T$  hadron spectrum [8]. Alternatively, models invoking thermal hadron production combined with collective transverse expansion of the reaction volume successfully describe the transverse momentum distributions of identified hadrons up to 3 GeV/c [10,11], which implies that the contribution of hard scattering would be negligible in this  $p_T$  range without explaining the origin of such a suppression. Another possibility is that the parton distributions in the incident gold nuclei are modified in such a way that the number of hard scatterings producing hadrons in the relevant  $p_T$  range is suppressed. Such nuclear modifications are well known [12] at both very low  $x$  (shadowing) and in the valence quark region  $0.3 < x < 0.8$ . But, in the  $p_T$  range covered by RHIC data at mid-rapidity, the dominant contributions are provided by partons in the so-called anti-shadowing region where quark distribution functions in nuclei are a few percent larger than in the nucleon and gluon distribution functions are thought to approach those of the nucleon [13–15].

An alternative picture for the modification of parton distributions in the nucleus at low- $x$  is provided by classical models of the initial gluonic content of a highly relativistic nucleus [16] and the radiation from these classical fields in a nuclear collision [17]. In these “saturation” models, the behavior of the low- $x$  gluons is controlled by a saturation scale,  $Q_s$ , that indicates where the evolution of the gluon distribution becomes non-linear. For  $p_T > Q_s$ , the hadron spectrum due to radiation from the classical fields reduces to the expression for gluon production in perturbative QCD processes [18,19]. However, effects of saturation on hadron spectra could occur for transverse momenta below  $Q_s$ , which according to recent estimates may be as large as 2 GeV/c in central Au+Au collisions at RHIC [20]. One robust prediction of the saturation model is that gluon  $p_T$  spectra scale with  $Q_s$  [19]. Since  $Q_s$  increases with the number of nucleons participating in the collision ( $N_{part}$ ), we would expect the hadron  $p_T$  spectra to broaden with increasing  $N_{part}$  in a saturation-dominated  $p_T$  range.

The previously published high- $p_T$  data [5] do not provide enough information to exper-

imentally determine the centrality region over which the suppression of the high- $p_T$  yield sets in. To address this problem and to provide more experimental constraints on theoretical descriptions of the high- $p_T$  suppression we present the centrality dependence of semi-inclusive charged hadron spectra measured by the PHENIX experiment over the range  $0.5 < p_T < 5.0$  GeV/c. The measurements are obtained from  $1.4 \times 10^6$  minimum bias Au+Au collisions at  $\sqrt{s_{NN}}=130$  GeV recorded during the Run-1 operation of RHIC (August - September 2000). Details on the PHENIX detector and its configuration in Run-1 operation can be found in [5,21].

## II. EXPERIMENTAL SETUP AND DATA ANALYSIS

The charged particles are measured in the east central arm spectrometer of PHENIX using data from a drift chamber (DC) and two segmented cathode pad chambers (PC1 and PC3). The detectors cover an azimuthal acceptance of  $90^\circ$  and a pseudo-rapidity range of  $|\eta| < 0.35$ . A fiducial cut of  $|\eta| < 0.18$  was applied in the analysis to guarantee homogeneous track acceptance for collisions within  $\pm 30$  cm of the nominal interaction point along the beam direction. A time-of-flight counter about five meters from the vertex allows proton identification over approximately one forth of the azimuthal coverage of the east arm. The flight times are measured with a resolution of  $\sigma = 115$  ps allowing to identify protons well above 3.5 GeV where at present the analysis of proton and anti-proton spectra are limited by statistics.

A track within the acceptance is reconstructed from the DC measurements of its trajectory projected into the bend plane of the PHENIX axial magnetic field matched to space-points provided by PC1 and PC3. This tracking system determines the momentum resolution of  $\delta p/p \simeq 0.6\% \oplus 3.6\% p$  (GeV/c). Each track is required to point back to the event vertex within 2.5 cm along the beam direction as reconstructed from two beam-beam counters. This cut removes most physical background from decays in flight and photon conversions close to the DC which mimic high momentum tracks. The level of remaining

background contamination in the charged track sample is negligible below 4 GeV/c, and below 30% at 5 GeV/c. This upper estimate of the remaining background is included in the systematic errors. The unphysical background in the charged particle sample, resulting from false associations of drift chamber projections with pad chamber points, is estimated and subtracted by forming artificial events with the locations of pad chamber points inverted around the symmetry axis of the spectrometer.

The data are corrected for geometrical detector acceptance and inhomogeneous detector performance, as well as for reconstruction efficiency, for decays in flight, and for the effects of finite momentum resolution. The correction function is obtained by tracing individual particles through a full GEANT simulation of the detector. The simulated detector response is embedded into real events. The resulting events are reconstructed using the full analysis chain to determine the effects of detector occupancy.

The average track reconstruction efficiency is larger than 98% in peripheral collisions and decreases to  $68 \pm 6\%$  for central collisions. The centrality dependence of the corresponding correction, including systematic errors, is shown on the upper left hand side of Fig. 1. The full correction depends on  $p_T$ , it is plotted for peripheral collision on the upper right hand side of the figure. Between 0.8 and 2.5 GeV/c the correction factor varies only slowly with  $p_T$ . Its value of  $\sim 25$  can easily be understood in terms of acceptance ( $\Delta\phi = \pi/4$ ;  $\Delta\eta = 0.36$ ), dead areas of the detectors ( 45% DC, 5% PC's), and losses due to  $2\sigma$  track matching cuts. At lower  $p_T$  the correction increases reflecting the gradual loss of acceptance. At higher  $p_T$  the correction function decreases to compensate for finite momentum resolution. At the end of our  $p_T$  coverage (5 GeV/c) the correction is reduced by  $\sim 50\%$ . The dashed lines indicate a conservative estimate of the systematic uncertainties of these corrections. The systematic uncertainties are tabulated in Tab.I for different  $p_T$ . Over the measured range, the  $p_T$  variation of the correction function is independent of the detector occupancy and thus of the event centrality. The ratio of the  $p_T$  dependent correction functions for central and peripheral collisions is constant with high accuracy. We estimated that between 2 and 5 GeV/c the  $p_T$  dependence of the correction changes by less than 2% at a  $3\sigma$  level.

Events are selected according to centrality following the procedure described in [5]. Events are classified by the energy measured in two zero-degree calorimeters ( $E_{ZDC}$ ) and the number of charged-particles detected in two beam-beam counters ( $N_{BBC}$ ). Six exclusive centrality bins are established by cuts in the  $E_{ZDC}$ - $N_{BBC}$  plane. A Glauber model based Monte-Carlo simulation which includes the zero-degree calorimeter and beam-beam counter response was used to estimate the average number of binary nucleon-nucleon collisions ( $N_{binary}$ ) and the corresponding average number of participating nucleons ( $N_{part}$ ) for each bin. The results including systematic errors are quoted in Tab. II. Throughout the paper we will characterize event centrality by  $N_{part}$ .

### III. RESULTS

Invariant charged hadron  $p_T$  spectra are presented in Fig. 2 for the six centrality bins. Only statistical errors are shown. The  $p_T$  dependent systematic errors, which are given in Tab. I, are independent of centrality. The centrality dependent errors are less than 10% and small compared to the symbol size.

To compare the shapes of the spectra from the different centrality classes we also plot in Fig. 2 the ratio of the differential yields in each centrality bin to the minimum-bias spectrum. Due to the strong growth in particle yield with centrality the shape of the minimum-bias spectrum is dominated by central collisions so the ratios for the central bins are flat with  $p_T$ . The peripheral bins show a decreasing ratio between 0.5 and 1.5 GeV/c indicating that the yield in this region grows less rapidly with increasing  $p_T$  than in central collisions. However, the ratio starts to rise again above 1.5 GeV/c indicating a proportionately higher yield in peripheral collisions in this  $p_T$  region.

The interpretation of charged hadron spectra at high  $p_T$  is complicated by the proportionally large yield of protons and anti-protons [22]. For  $p_T > 2$  GeV/c the proton and anti-proton yields become comparable to the pion yield. Since these (anti-)protons do not necessarily arise from hard scattering processes, they may be a source of “background” to

the hard scattering contributions in the high- $p_T$  charged hadron spectra. To evaluate the effect of including the (anti-)protons, we plot in the top panel of Fig. 3 the  $p_T$  dependence of  $p/h$ , the ratio of proton plus anti-proton yields, to the total charged hadron yield for minimum bias collisions. This ratio increases steadily up to 1.5 GeV/c, from then on it saturates reaching a value of  $\sim 0.5$  around 3.0 GeV/c. In the bottom panel of Fig. 3 we show  $p/h$  for  $p_T$  above 1.8 GeV/c as a function of centrality. Since the relative contribution of (anti-)protons to the hadron spectra grows by 20-30% with increasing  $N_{part}$ , we may over-estimate the growth of the hard scattering contributions to the high  $p_T$  hadron spectra with increasing  $N_{part}$  by this same factor.

We have seen in Fig. 2 that the charged hadron spectra change in shape with collision centrality. To evaluate this change more quantitatively we calculate the truncated average  $p_T$ :

$$\langle p_T^{trunc} \rangle \equiv \frac{\int_{p_T^{min}}^{\infty} p_T \cdot dN/dp_T}{\int_{p_T^{min}}^{\infty} dN/dp_T} - p_T^{min} \quad (3.1)$$

for  $p_T^{min} = 0.5$  GeV/c and for  $p_T^{min} = 2.0$  GeV/c for each centrality selection. In Fig. 4  $\langle p_T^{trunc} \rangle$  is plotted<sup>1</sup> as a function of  $N_{part}$ . Since the value of  $\langle p_T^{trunc} \rangle$  is insensitive to the normalization of the spectra, the primary systematic uncertainty results from an 1-2% uncertainty on the momentum scale. It is essentially independent of centrality at values of  $\sim 20$  and  $\sim 50$  MeV/c for  $p_T^{min} = 0.5$  and 2 GeV/c, respectively. The  $p_T$  dependent uncertainties of the correction function contribute an additional uncertainty of 8 MeV/c to the systematic error.

The  $\langle p_T^{trunc} \rangle$  for  $p_T^{min} = 0.5$  GeV/c increases with  $N_{part}$  similar to the average transverse momentum of identified charged particles [22]. By contrast,  $\langle p_T^{trunc} \rangle$  for  $p_T^{min} = 2.0$  GeV/c drops with  $N_{part}$  by about 60 MeV/c. For the most central collisions the two values differ by only  $\sim 10$  MeV/c. The decreasing  $\langle p_T^{trunc} \rangle$  values in the high  $p_T$  region indicates a decrease

---

<sup>1</sup> Note that the relation of  $\langle p_T^{trunc} \rangle$  to the local slope is non trivial. For the simple case of an exponential spectrum the conversion depends on  $p_T^{min}$ . For an exponential with an inverse slope of 350 MeV the correction is approximately -80 (-60) MeV/c for  $p_T^{min} = 0.5(2.0)$  GeV/c.

of the inverse slope of the spectrum at high  $p_T$  with increasing  $N_{part}$ .

Because of factorization and the small cross-sections, hard-scattering rates in nucleus-nucleus collisions are expected to increase proportional to  $N_{binary}$  if medium modifications can be ignored. In nucleon-nucleon (N+N) collisions the single hadron spectra above  $p_T = 2$  GeV/c are dominated by the hard scattering contributions. Thus, we would expect that in nucleus-nucleus collisions the yield of hadrons above 2 GeV/c should grow at least as fast as  $N_{binary}$ . However, we observe that with increasing  $N_{part}$  the high- $p_T$  particle yield drops more rapidly with  $p_T$ , suggesting a relative reduction of the hard scattering contribution.

Changes of the spectrum at high  $p_T$  are often evaluated by the nuclear modification factor,  $R_{AA}$ , defined by:

$$R_{AA}(p_T, \eta) = \frac{1}{N_{evt}} \frac{d^2 N^{A+A}}{dp_T d\eta} / \frac{\langle N_{binary} \rangle}{\sigma_{inel}^{N+N}} \frac{d^2 \sigma^{N+N}}{dp_T d\eta}. \quad (3.2)$$

We have calculated  $R_{AA}$  for each centrality bin. We use a power-law parameterization for the N+N charged hadron cross section  $1/\pi d^2\sigma/dp_T^2 = A/(1 + p_T/p_0)^n$ , with  $A = 330$  mb/(GeV/c) $^2$ ,  $p_0 = 1.72$  GeV/c, and  $n=12.4$ . The parameters were obtained by interpolating p+p and  $\bar{p}$ +p data to  $\sqrt{s} = 130$  GeV as described in [5]. In Fig. 5 the  $R_{AA}(p_T)$  values for all centrality bins excluding the most peripheral one are compared to the most central bin. Comparing two centrality bins, the systematic errors are dominated by the uncertainty in  $N_{binary}$  (listed in Table II). For more central collisions uncertainties in the reconstruction efficiency also contribute. Relative to the most central bin the errors increase from  $\sim 6\%$  for bin 5 (5-15%) to nearly 27% for bin 2 (60-80%). These errors are indicated by the brackets on the  $R_{AA}$  data points for the more peripheral sample on each panel. In addition to the uncertainty in  $N_{binary}$ , systematic errors in the normalization of the data (see Tab. I) and in the N+N reference (20-35%) result in a larger overall systematic error on the  $R_{AA}$  scale. For the range  $1.0 < p_T < 3.5$  GeV/c the errors are about 41%, 34%, 31%, 31% and 30% for centrality bins 2-6 respectively. They are indicated on the left side of each panel by a solid bar centered around unity. At higher  $p_T$  the uncertainty is larger by a few percent.

The  $R_{AA}$  values confirm that at high  $p_T$  the yield of hadrons relative to the expected hard-scattering contribution decreases in more central collisions. For the second centrality bin (60-80%),  $R_{AA}$  increases with  $p_T$  and reaches unity at high  $p_T$ . In comparison to the 60-80% bin, the  $R_{AA}$  values for the most central bin remain significantly below unity at a value of 0.55 for  $p_T > 2$  GeV/c. A saturation in the  $R_{AA}$  values at high  $p_T$  is detected in all centrality bins. The saturation value decreases monotonically with centrality clearly indicating that the magnitude of the suppression of high  $p_T$  hadrons increases with centrality. Most of the suppression seems develops over the 30-60% centrality bin corresponding to 40-140 participating nucleons, while for the 30% most central collisions the suppression changes by only 15%.

We note that the data do not indicate a significant increase of  $R_{AA}$  above unity, unlike data at lower energies [23]. However, such an increase, attributed to initial state scattering, the Cronin effect [24], may well be consistent with the peripheral data due to the large systematic uncertainty of the  $R_{AA}$  scale. While the relative difference between the peripheral and central spectra increases with  $p_T$ , the saturation of the nuclear modification factor at large  $p_T$  suggests an approximately  $p_T$  independent suppression of hard scattering contributions over the range  $2 < p_T < 4.5$  GeV/c.

To characterize the centrality dependence of the high- $p_T$  hadron suppression, we plot in Fig. 6 (top panel)  $R_{AA}$  averaged over three  $p_T$ -intervals, 1.6 to 2.6 GeV/c, 2.6 to 3.6 GeV/c, and above 3.6 GeV/c as a function of  $N_{part}$ . Only statistical errors are shown. The systematic error on the scale is identical to the scale error shown in Fig. 5. Each data point has centrality dependent systematic errors given by the brackets in Fig. 5, which are dominated by the uncertainty of both  $N_{part}$  and  $N_{binary}$  in peripheral collisions. These errors are correlated, i.e. take their maximum or minimum value simultaneously for all centrality and  $p_T$  selections. In addition, there are also  $p_T$  dependent systematic errors, which are given in Tab. I. The systematic errors do not alter the trends in the data.

For all  $p_T$  selections  $R_{AA}$  decreases with centrality. For central collisions and increasing  $p_T$  the values are 4/5, 2/3, and 1/2 of the value observed in peripheral collisions. While

$R_{AA}$  increases with  $p_T$  for peripheral events it seems to decrease for central collisions. The trend is reversed over the 30-60% centrality bin.  $R_{AA}$  for the lowest  $p_T$  bin remains below unity at all  $p_T$ . Because this bin extends below 2 GeV/c it includes soft particle production and even in the absence of nuclear modifications to hard processes it would not *a priori* be expected that the yield increases proportional to  $N_{binary}$ .

The physics that controls the production of high- $p_T$  particles or the suppression of the hard scattering yields in the measured  $p_T$  range may not depend directly on  $N_{binary}$ . Thus, we have calculated a different ratio,  $R_{AA}^{part}$ , defined similar to  $R_{AA}$  but with  $N_{binary}$  replaced by the number of participant pairs,  $N_{part}/2$ . If particle production increases proportional to the number of participants,  $R_{AA}^{part} = 1$ .

The obtained  $R_{AA}^{part}$  values are shown in Fig. 6 (bottom) for the three  $p_T$  bins used above. The values in the bottom panel in Fig. 6 are larger than in the top panel by a factor equal to  $N_{coll}/N_{part}$  the average number of nucleon-nucleon collisions suffered by each participant. For all  $p_T$  bins the yield per participant is consistent with one for peripheral collisions as expected since peripheral collisions should closely resemble N+N collisions. For central collisions  $R_{AA}^{part}$  increases approximately to a value of three. Most of this change occurs in the range of  $N_{part}$  from 40 to 140. The saturation of  $R_{AA}^{part}$  occurs at lower values of  $N_{part}$  for larger  $p_T$ . For larger  $N_{part}$  the yield in the highest  $p_T$  bin is approximately constant while in both lower  $p_T$  bins it increases by 20 to 30%.

#### IV. CONCLUDING DISCUSSION

In this paper we have presented measurements of the centrality dependence of charged hadron  $p_T$  spectra focusing on the behavior of the spectra at high  $p_T$ . A striking change of the spectral shape is observed when comparing spectra from different centrality selections. For peripheral collisions the spectrum exhibits a pronounced power-law shape which is modified towards a more exponential spectrum as the centrality increases. This change is not related to the large proton contribution to the charged particle yield above 2 GeV/c.

We observe a decrease of  $\langle p_T^{trunc} \rangle$  for  $p_T > 2$  GeV/c with increasing centrality, which is distinctly different from the increase of  $\langle p_T \rangle$ . This result is challenging for scenarios that do not include energy loss of hard scattered partons in a dense medium. Without energy loss, particle production from hard scattering processes should increase relative to soft production by the factor  $N_{coll}/N_{part}$  which grows from 1.5 to  $\sim 6$  from peripheral to central collisions. Thus for large  $p_T^{min}$  the value of  $\langle p_T^{trunc} \rangle$  should increase due to the increased strength in the power-law contribution to the  $p_T$  spectrum. Also if the  $p_T$  spectra above 2 GeV/c are strongly affected by collective motion of matter before freeze-out, we would expect an increase  $\langle p_T^{trunc} \rangle$  since the corresponding flow velocities should increase in more central collisions [26]. Similarly, if gluon saturation is important for particle production in the  $p_T$  range above 2 GeV/c,  $\langle p_T^{trunc} \rangle$  should increase with increasing  $N_{part}$  due to the predicted logarithmic increase of  $Q_s$  [25]. On the other hand, energy loss of hard scattered partons predicts a reduction of the hard scattering contribution to the hadron spectrum, which becomes more pronounced in central collisions in qualitative agreement with the data [6,7,9]. It remains to be seen whether this explanation is unique or if other models of energy loss by collisions with cold or hot nuclear matter [8] can also explain the data.

Comparing the measured differential yields in five centrality bins to an  $N_{binary}$  scaling of the N+N reference yields we see a suppression of the yields in central collisions at high  $p_T$ , consistent with the results in [5]. In the 0-30% centrality range (bins 1-3) the suppression is approximately independent of  $p_T$  for  $2 < p_T < 5$  GeV/c at a value of  $R_{AA} \sim 0.6$  and simultaneously nearly independent within 20% of centrality. This behavior is consistent with parton energy loss scenarios if there is a cancellation between a Cronin enhancement and parton energy loss [23]. In these calculations, the value of  $R_{AA}$  in the measured  $p_T$  range and the shape of  $R_{AA}$  at higher  $p_T$  is very sensitive to the actual energy loss prescription. Due to the large systematic errors on the  $R_{AA}$  scale, contamination from the protons and the limited  $p_T$  reach of the data presented here, we can not distinguish between the different energy loss prescriptions on the basis of  $R_{AA}$ .

By contrast, for the 60-80% centrality bin  $R_{AA}$  increases with  $p_T$  and reaches unity

near 3 GeV/c. This is consistent with the expected dominance of hard processes above 2 GeV/c and a potential enhancement of the high  $p_T$  yield similar to the Cronin effect. The suppression of  $R_{AA}$  at high  $p_T$  occurs over the 30-60% centrality bin, which covers a large range of collision geometries. Whether the change is continuous or exhibits a threshold behavior, like predicted in [27], can not be judged from the present data. A more detailed analysis of this region with higher statistics will be very interesting.

In summary, a detailed analysis of the centrality dependence of charged particle data from Au-Au collisions at  $\sqrt{s_{NN}} = 130$  GeV measured by PHENIX reveals interesting features of the observed high  $p_T$  hadron suppression. The decrease of the average  $p_T > 2$  GeV/c with increasing centrality seems to favor models of particle production that consider parton energy loss effects, rather than saturation- or hydrodynamical- based approaches for this  $p_T$  range. The suppression sets in over the centrality range from 30-60% corresponding to about 40-140 nucleons participating in the collision and from there on does not change substantially towards more central collisions.

We thank the staff of the Collider-Accelerator and Physics Departments at BNL for their vital contributions. We acknowledge support from the Department of Energy and NSF (U.S.A.), MEXT and JSPS (Japan), RAS, RMAE, and RMS (Russia), BMBF, DAAD, and AvH (Germany), VR and KAW (Sweden), MIST and NSERC (Canada), CNPq and FAPESP (Brazil), IN2P3/CNRS (France), DAE and DST (India), KRF and CHEP (Korea), the U.S. CRDF for the FSU, and the US-Israel BSF.

## REFERENCES

\* Deceased

- [1] J.A. Appel et al., Phys. Rev. **D20** (1979) 53.
- [2] M. Gyulassy and M. Plümer, Phys. Lett. **B243** (1990) 432; X.N. Wang and M. Gyulassy, Phys. Rev. Lett. **68** (1992) 1480.
- [3] X.N. Wang, M. Gyulassy and M. Plümer, Phys. Rev. **D51** (1995) 3436; R. Baier et al., Phys. Lett. **B345** (1995) 277; R. Baier, D. Schiff and B.G. Zakharov, Ann. Rev. Nucl. Part. Sci. **50** (2000) 37-69.
- [4] M. Gyulassy and X.N. Wang, Nucl. Phys. **B420** (1994) 583; X.N. Wang, Phys. Rev. **C58** (1998) 2321.
- [5] PHENIX Collaboration, K. Adcox et al., Phys. Rev. Lett. **88** (2002) 22301.
- [6] X.N. Wang Phys. Rev. **C61** (2000) 64910.
- [7] M. Gyulassy, P. Levai and I. Vitev, Phys. Rev. Lett. **85** (2000) 5535.
- [8] K. Gallmeister, C. Greiner, and Z. Xu, nucl-th/0202051.
- [9] P. Levai et al., Nucl. Phys. **A698** (2002) 631.
- [10] P. Kolb et al., Nucl. Phys. **A696** (2001) 197.
- [11] D. Teaney, J. Lauret and E.V. Shuryak, nucl-th/0110037.
- [12] J.J. Aubert et al., Phys. Lett. **B123**, (1983) 275.
- [13] L.V. Gribov, E.M. Levin and M.G. Ryskin, Phys. Repts. **100** (1983) .
- [14] Z. Huang, H. J. Lu and I. Sarcevic, Nucl. Phys. **A637** (1998) 79.
- [15] K.J. Eskola, V.J. Kolhinen and C.A. Salgado, Eur.Phys.J. **C9** (1999) 61.
- [16] L. D. McLerran and R. Venugopalan, Phys. Rev. **D49** (1994) 2233.

- [17] A. Kovner, L. D. McLerran and H. Weigert, Phys. Rev. **D52** (1995) 6231.
- [18] M. Gyulassy and L. D. McLerran, Phys. Rev. **C56** (1997) 2219.
- [19] A. Krasnitz, Y. Nara and R. Venugopalan, Phys. Rev. Lett. **87** (2001) 192302.
- [20] D. Kharzeev and M. Nardi, nucl-th/0012025 and references therein.
- [21] K. Adcox et al., Phys. Rev. Lett. **86** (2001) 3500. K. Adcox et al., Phys. Rev. Lett. **87** (2001) 052301.
- [22] K. Adcox et al., nucl-ex/0112006.
- [23] E. Wang and X. N. Wang, nucl-th/0104031 and references therein.
- [24] D. Antreasyan *et al.*, Phys. Rev. **D19** (1979) 764.
- [25] D. Kharzeev and E. Levin, nucl-th/0108006, J. Schaffner-Bielich et al., nucl-th/0108048.
- [26] E. Shuryak private communication.
- [27] X.N. Wang, Phys. Rev. **C63** (2001) 54902.

## FIGURES

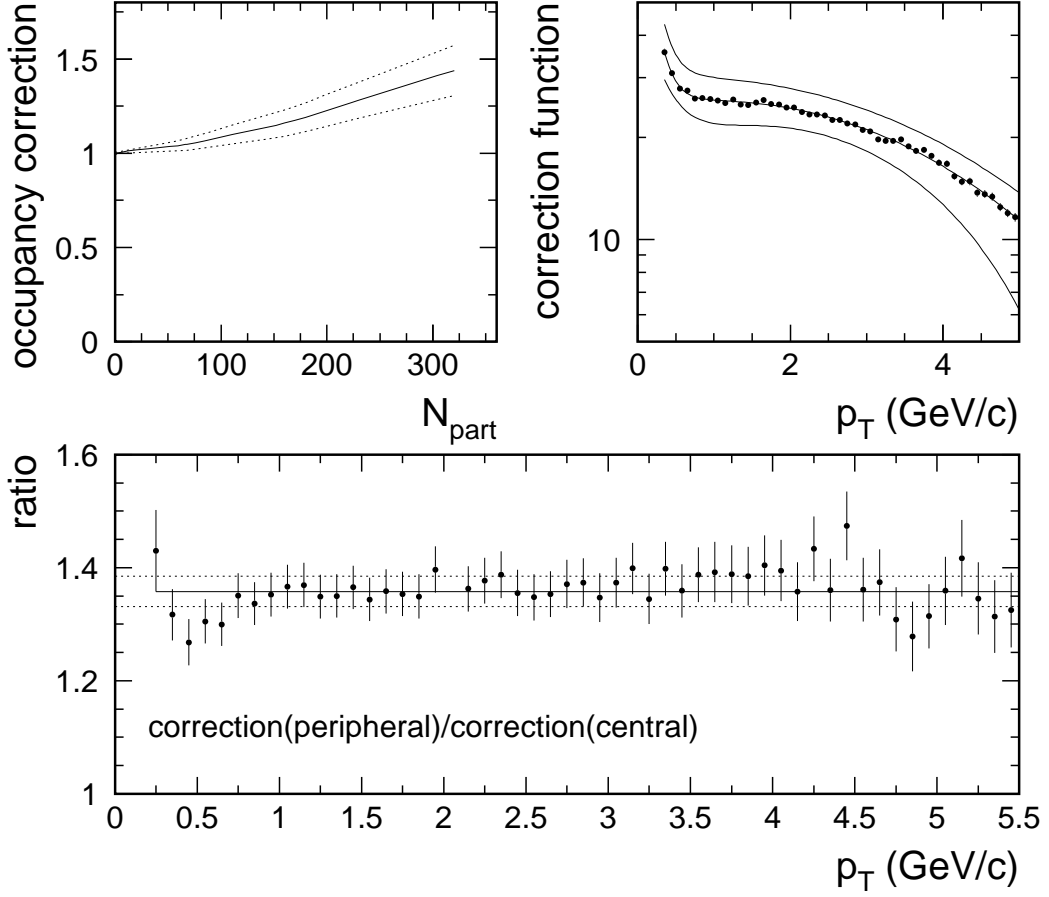


FIG. 1. Functions used to correct the charged particle  $p_T$  spectra. Upper left panel shows the centrality dependent correction  $c(N_{part})$ . The figure on the left shows  $c(p_T)$  the correction for a single particle in the detector as function of  $p_T$ . The dashed lines indicate the systematic uncertainties (see text for details). For any give centrality the final correction function is calculated as product  $c(p_T) \times c(N_{part})$ . The accuracy of this factorisation of centrality and  $p_T$  dependence of the correction is demonstrated in the lower panel. The ratio of the correction for central collisions (top 5%) to the correction for single particles varies by less than 2% above 1 GeV/c.

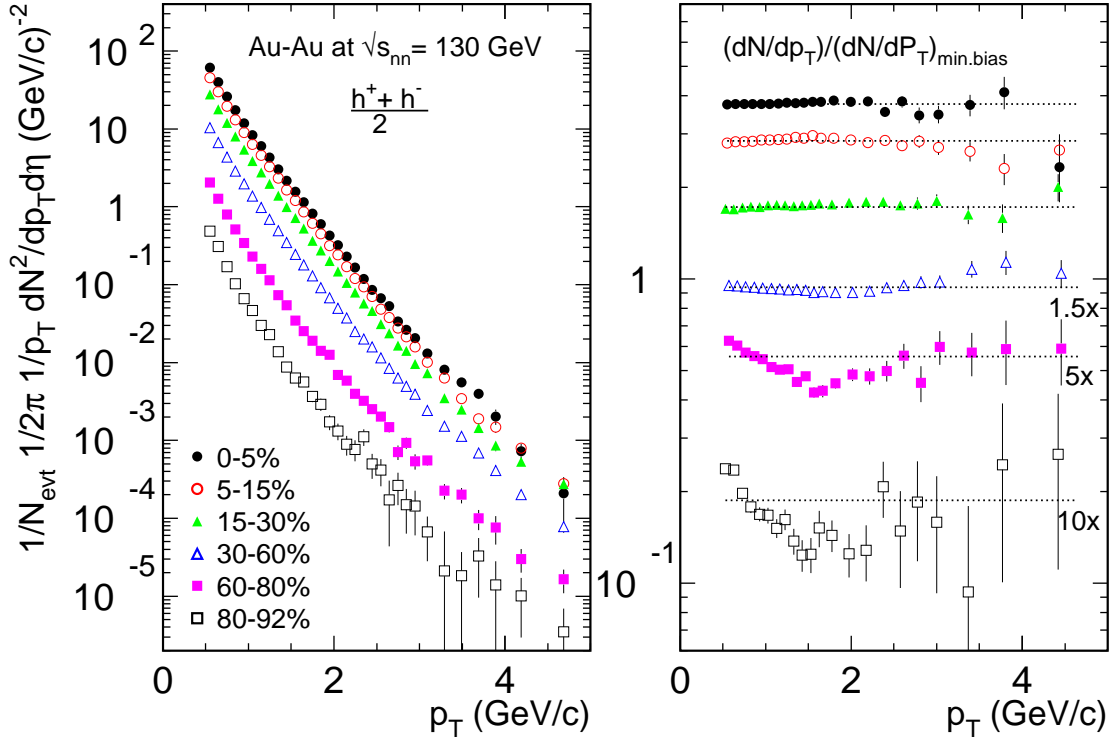


FIG. 2. The left panel shows  $p_T$  spectra of charged hadrons from six Au+Au centrality selections. Error bars indicate statistical errors only. The right panel shows the ratio of each of the centrality selected  $p_T$  spectra to the minimum bias spectrum. Ratios for peripheral selections are scaled for clarity. Dotted lines indicate the average ratios for each centrality selection.

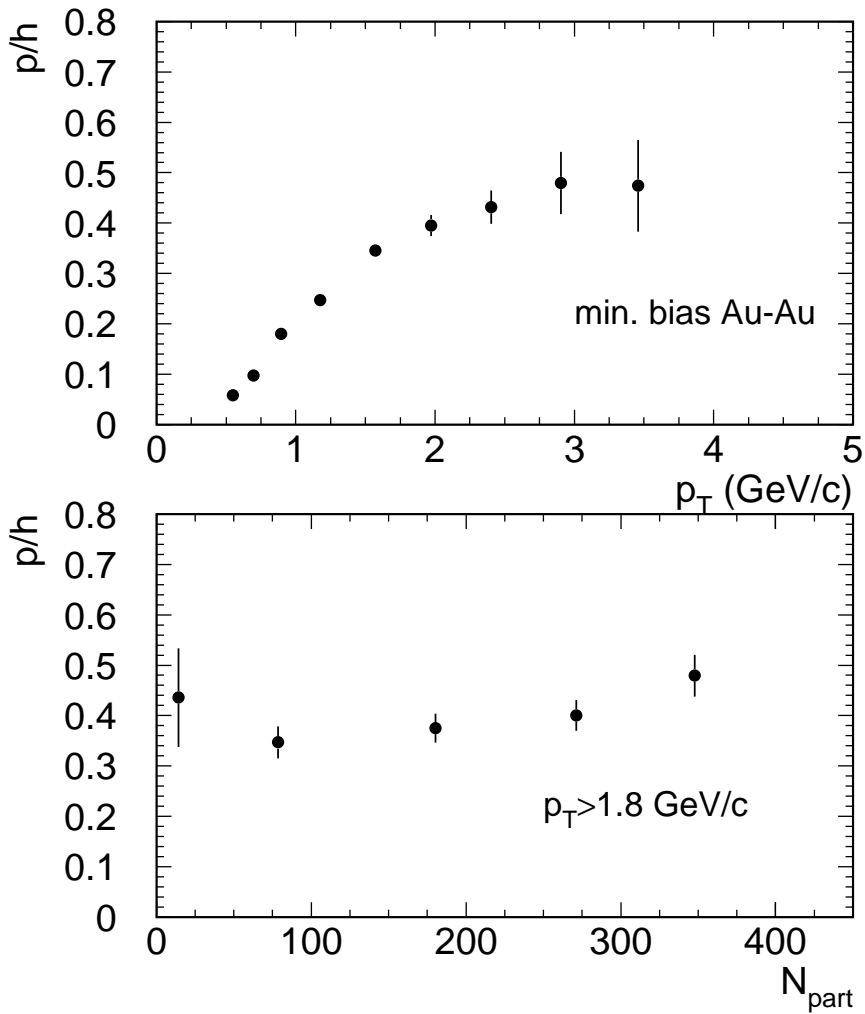


FIG. 3. The ratio  $p/h$  represents the proton plus anti-proton yield relative to the total charged hadron multiplicity. The top panel shows the  $p_T$  dependence of  $p/h$  for minimum bias events. In the bottom panel we show the centrality dependence of  $p/h$  for  $p_T > 1.8$  GeV/c. Only statistical errors are shown.

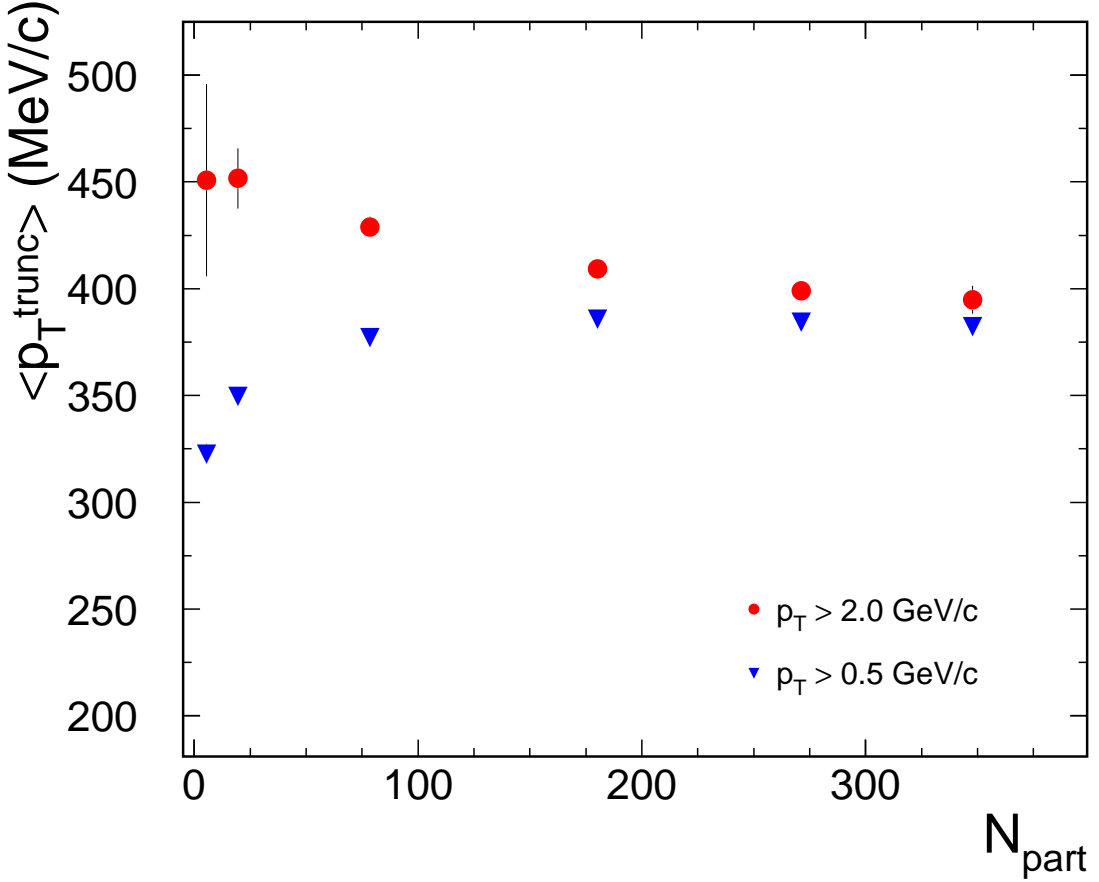


FIG. 4. Centrality dependence of  $\langle p_T^{\text{trunc}} \rangle$ , the average  $p_T$  of charged particles with  $p_T$  above a threshold  $p_T^{\text{min}}$  minus the threshold  $p_T^{\text{min}}$ . Shown are values for two  $p_T^{\text{min}}$  cuts, one at  $p_T > 0.5 \text{ GeV}/c$  representing all data presented in Fig. 2 and the other one at  $p_T > 2 \text{ GeV}/c$ . Only statistical errors are shown.

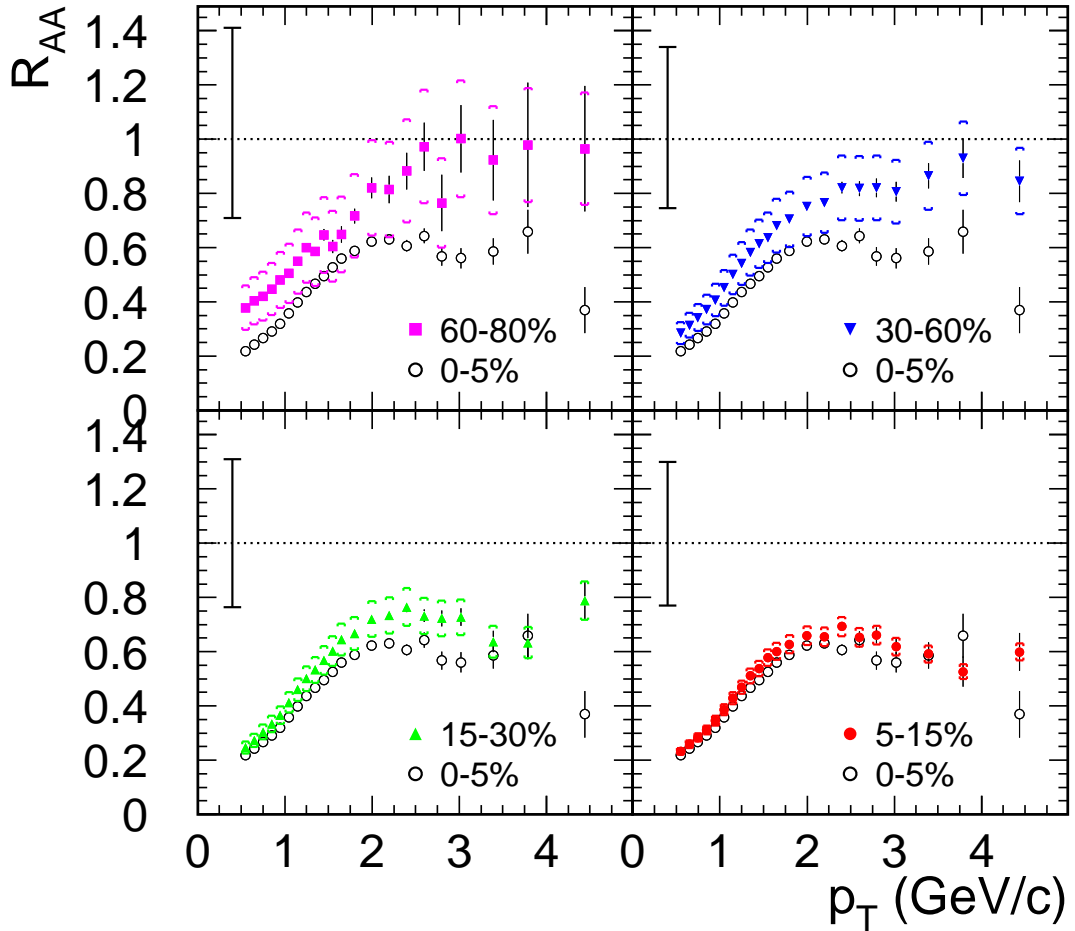


FIG. 5. Nuclear modification factor ( $R_{AA}$ ) for the 60-80%, 30-60%, 15-30%, and 5-15% centrality selections compared to the one for the most central sample (0-5%). Due to insufficient statistics  $R_{AA}$  is not shown for the 80-92% sample. The solid error bars on each data point are statistical. The systematic error between the more peripheral and the central sample are given as brackets for the more peripheral data points. The error bar on the left hand side of each panel indicates the overall systematic error on the  $R_{AA}$  scale.

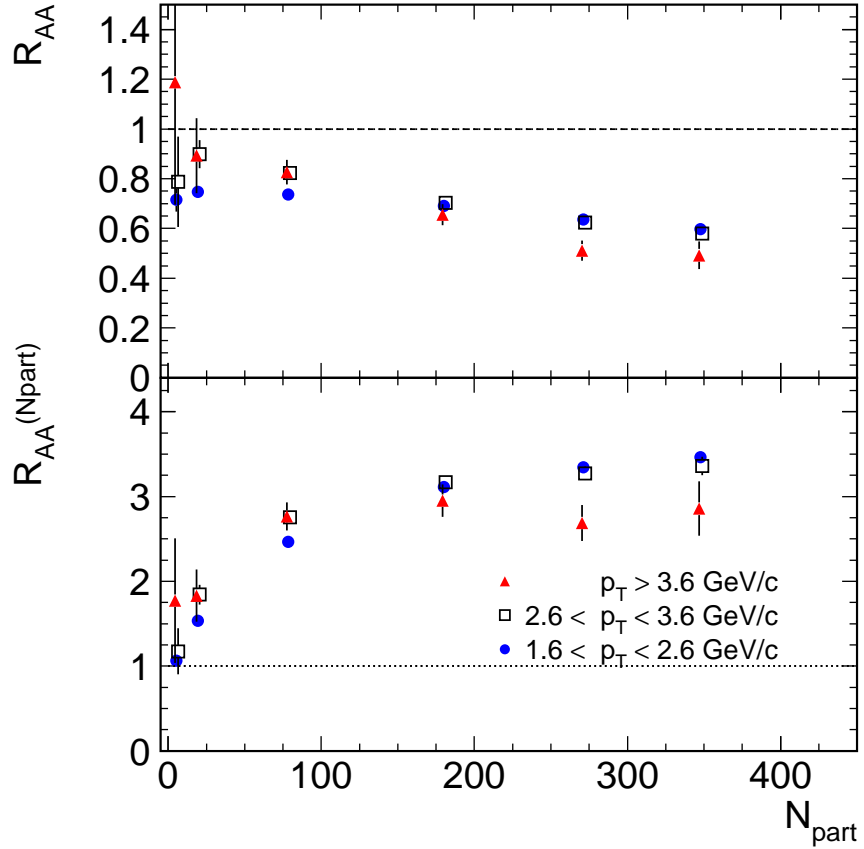


FIG. 6. The top panel gives the nuclear modification factor  $R_{AA}$  for three exclusive  $p_T$  regions as a function of the centrality of the collision. The lower panel shows essentially the same quantity but normalized to the number of participant pairs rather than to the number of binary collisions. The dotted line indicates the expectation for scaling with the number of binary collisions (top) or with the number of participants (bottom). Only statistical errors are shown. The systematic uncertainties are discussed in the text.

## TABLES

$p_T$ (GeV/c)	$\delta_{track}$ (%)	$\delta_{decay}$ (%)	$\delta_{reso}$ (%)	$\delta_{bgr}$ (%)	total
1	$\pm 13.5$	+ 10	$\pm 0$	0	-13.5 +16.4
2	$\pm 13.5$	+ 5	$\pm 1$	0	-13.7 +14.4
3	$\pm 13.5$	+ 2.5	$\pm 4$	-1.6	-14.2 +14.2
4	$\pm 13.5$	+ 1.25	$\pm 9$	-11.5	-20 +16
5	$\pm 13.5$	+ 0.6	$\pm 15$	-15	-45 +20

TABLE I. Conservative upper estimates of the systematic error on the  $p_T$  dependent single particle correction function. Here  $\delta_{track}$  includes the uncertainties of the acceptance, dead areas, track matching cuts and the track reconstruction efficiency. The  $\delta_{decay}$  term accounts for the uncertainty of the decay correction. The effect of the momentum resolution contributes with  $\delta_{reso}$  to the systematic error. Uncertainties due to potentially unsubtracted background are quantified by  $\delta_{bgr}$ . The total systematic error given in the last column is calculated as quadrature sum of the individual contributions. It is calculated separately for positive and negative errors.

bin	relative fraction	$N_{part}$	$N_{binary}$	$N_{binary}^{central} / N_{binary}$	$N_{coll} / N_{part}$
1	80-92%	$5.5 \pm 2.6$	$4.1 \pm 1.7$	$246 \pm 98$	1.5
2	60-80%	$19.5 \pm 3.5$	$20 \pm 6$	$50.4 \pm 13$	2.1
3	30-60%	$79 \pm 4.6$	$131 \pm 23$	$7.68 \pm 1.1$	3.4
4	15-30%	$180 \pm 6.6$	$406 \pm 46$	$2.49 \pm 0.13$	4.5
5	5-15%	$271 \pm 9$	$712 \pm 72$	$1.41 \pm 0.03$	5.2
6	0-5%	$348 \pm 10$	$1009 \pm 101$	1	5.8

TABLE II. Number of participants and binary collisions and their systematic errors for the individual centrality selections used in this analysis. Also given is the ratio of the number of binary collisions for each sample relative to the most central sample. The last column quantifies the ratio of binary collisions to participant pairs.